A data fusion system of GNSS data and on-vehicle sensors data for improving car positioning precision in urban environments

Carlos Melendez-Pastor [1,†], Ruben Ruiz-Gonzalez [1,*,†], and Jaime Gomez-Gil [1,†]

[1] Department of Signal Theory, Communications and Telematics Engineering, University of Valladolid, Valladolid 47011, Spain; E-Mails: cmelpas@ribera.tel.uva.es (C.M.-P.); jgomez@tel.uva.es (J.G.-G.)

[†] These authors contributed equally to this work.

***** Author to whom correspondence should be addressed; E-Mail: rruigon@ribera.tel.uva.es; Tel.: +34-6366-81022; Fax: +34-9834-23667.

Abstract:

Accurate car positioning on the Earth's surface is a requirement for many state-of-the-art automotive applications, but current low-cost Global Navigation Satellite System (GNSS) receivers can suffer from poor precision and transient unavailability in urban areas. In this article, a real-time data fusion system of absolute and relative positioning data is proposed with the aim of increasing car positioning precision. To achieve this goal, a system based on the Extended Kalman Filter (EKF) was employed to fuse absolute positioning data coming from a low-cost GNSS receiver with data coming from four wheel speed sensors, a lateral acceleration sensor, and a steering wheel angle sensor. The bicycle kinematic model and the Ackerman steering geometry were employed to particularize the EKF. The proposed system was evaluated through experimental tests. The results showed precision improvements of up to 50% in terms of the Root Mean Square Error (RMSE), 50% in terms of the 95*th*-percentile of the distance error distribution, and 75% in terms of the maximum distance error, with respect to using a stand-alone, low-cost GNSS receiver. These results suggest that the proposed data fusion system for car vehicles can significantly reduce the positioning error with respect to the positioning error of a low-cost GNSS receiver. The best precision improvements of the system ~~can be~~are expected to be achieved in urban areas, where tall buildings hinder the effectiveness of GNSS systems. The main contribution of this work is the proposal of a novel system that enables accurate car positioning during short GNSS signal outages. This advance could be integrated in larger expert and intelligent systems such as autonomous cars, helping to make self-driving easier and safer.

Keywords: data fusion; Extended Kalman Filter (EKF); Global Navigation Satellite System (GNSS); on-vehicle sensors; On-Board Diagnostics (OBD); Ackerman steering geometry.

---

1. Introduction

Positioning technologies for locating a vehicle ~~over~~ on the Earth's surface are recurrently employed by applications such as Advanced Driver Assistance System (ADAS) (Pérez, et al., 2015) and vehicle navigation systems (Mintsis, Basbas, Papaioannou, Taxiltaris, & Tziavos, 2004). Vehicle positioning can rely exclusively on Global Navigation Satellite Systems (GNSSs) as the source of information to provide position and velocity. This absolute positioning technology can be accurate and highly available in environments with ~~a~~ good satellite visibility ~~of satellites~~. However, GNSS positioning precision can be degraded in urban environments, such as streets surrounded by high buildings, and the positioning can be canceled in environments such as tunnels (E. D. Kaplan & C. J. Hegarty, 2005; French, 1996).

Security systems in modern vehicles, such as Anti-lock Braking System (ABS), Electronic Stability Control (ESC), Traction Control System (TCS), and Electronic Brakeforce Distribution (EBD), use data from sensors located in different parts of the vehicle. Wheel speeds, steering wheel angle, lateral and longitudinal accelerations, vehicle rotation angular speed, and vehicle rotation angular acceleration are parameters continuously acquired and monitored in modern cars (Robert Bosch GmbH, 2007). The processing of these parameters coming from on-vehicle sensors enables relative positioning (Lin, 1991; Titterton & Weston, 2004).

The Extended Kalman Filter (EKF) (H. W. Sorenson, 1985; A. H. Jazwinski, 2007) allows the statistically optimal data fusion of absolute positioning data coming from GNSSs with data for relative positioning coming from on-vehicle sensors. Making use of the EKF, the positioning precision can be thus improved.

Among other applications, ~~The~~ the Kalman filter has been widely used in the literature~~, among other applications,~~ to (*i*) fuse data from Global Positioning System (GPS) and Inertial Navigation System (INS) (Tin Leung, Whidborne, Purdy, & Dunoyer, 2011); (*ii*) fuse data from GPS, INS, and Wheel Speed Sensors (WSS) (Leung, Whidborne, Purdy, & Barber, 2011); (*iii*) fuse data from GPS and positioning data obtained by artificial vision (Schleicher, Bergasa, Ocaña, Barea, & López, 2010); and (*iv*) smooth the path followed by vehicles (Gomez-Gil, Ruiz-Gonzalez, Alonso-Garcia, & Gomez-Gil, 2013). A line of research for the data fusion of low-cost GPS and on-vehicle sensors in cars was initiated in 1999 by Abbott and Powell (Abbott & Powell, 1999). Since then, more articles have been published in this line of research (Bonnifait, Bouron, Crubille, & Meizel, 2001; El Najjar & Bonnifait, 2005; Gning & Bonnifait, 2005; Song, Li, Tang, Zhang, & Li, 2014). The present article makes a new contribution to this same line of research by proposing an alternative approach for accomplishing the data fusion, as well as by proposing a different model for the car system's state.

This article proposes and experimentally evaluates an EKF-based data fusion system for improving car positioning precision. This system combines data from a low-cost GNSS receiver with data coming from six on-vehicle sensors: four wheel speed sensors, a lateral acceleration sensor, and a steering wheel angle sensor. As compared to the aforementioned articles in the related literature, the proposed system makes use of a different and modified model for the car system's state, not found in any previous related article, so far as the authors are aware~~up to the authors' knowledge~~.

2. Description of the Proposed System

2.1. Overview

The proposed data fusion system, whose main building blocks (Figure 1a) could be deployed in a microcontroller-based system, takes as input GNSS data, along with data for relative positioning coming from other on-vehicle sensors (Figure 1b). As far as this article is concerned, just the four wheel speed sensors, a lateral acceleration sensor, and a steering wheel angle sensor (Figure 1b) were employed for relative positioning, along with a GNSS receiver for absolute positioning. Nevertheless, this does not preclude the incorporation of other relative positioning sensors, *e.g.* longitudinal accelerometers, which could be readily considered with few straightforward changes in the system architecture and its processing scheme.

The data supplied by the aforementioned sensors, following the scheme depicted in Figure 1a, is then preprocessed and, thereafter, ~~they are~~ combined via the Extended Kalman Filter. By taking into account all the redundant data, ~~This~~ this system provides~~, by taking into account all the redundant data,~~ a more precise estimation of the actual state of the vehicle.

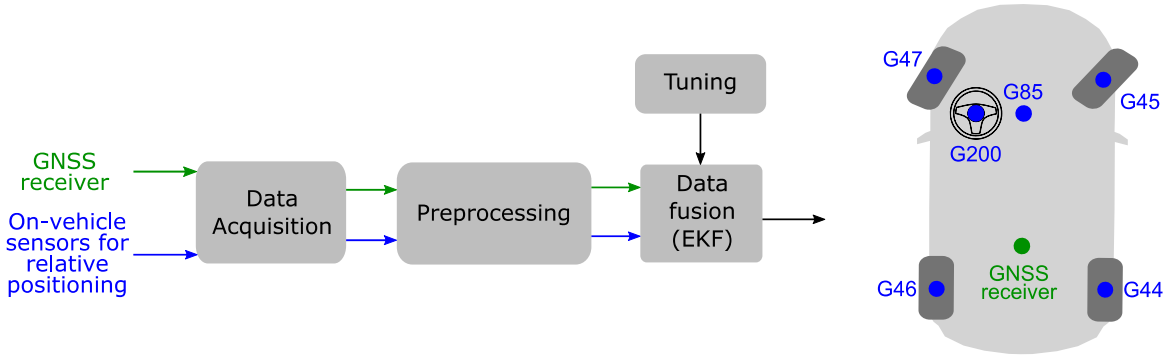

Figure 1. (**a**) Overview of the building blocks in the proposed system. (**b**) Location of the sensors employed in the proposed system. In green, the absolute positioning sensor: GNSS receiver. In blue, the on-vehicle sensors for relative positioning: wheel speed sensors (G44-G47), lateral acceleration sensor (G85), and steering wheel angle sensor (G200).

2.2. System building blocks

In this subsection, further details about the functioning of all the building blocks of the proposed system (Figure 1a) are provided.

2.2.1. Data Acquisition

The data acquisition block addresses the extraction of the raw data supplied by all the sensors from the system. Typically, RMC NMEA 0183 (National Marine Electronics Association 0183) sentences are acquired at a certain sampling rate from the GNSS receiver, and the raw data from the on-vehicle sensors for relative positioning is also obtained. This raw data is fed into the subsequent preprocessing block.

2.2.2. Preprocessing

The raw data, coming from the aforementioned sensors, must be preprocessed in order to obtain meaningful and comparable data for the subsequent data fusion step. This preprocessing block requires the performance of several actions, which can be conceptually encompassed ~~englobed~~ in the following two steps: (*1*) The conversion of the raw data and electric signals provided by the sensors into the meaningful variables depicted in Figure 2. This step includes the conversion from GNSS geodetic coordinates to the Universal Transverse Mercator (UTM) planar projection as well as other basic conversions, such as converting every involved variable into SI units. (*2*) The synchronization, resampling, and interpolation of the acquired data so that all the digital samples from each sensor correspond to the same temporal instant.

The output data from this preprocessing block is the set of measured variables represented in Figure 2, which is fed into the subsequent data fusion block.

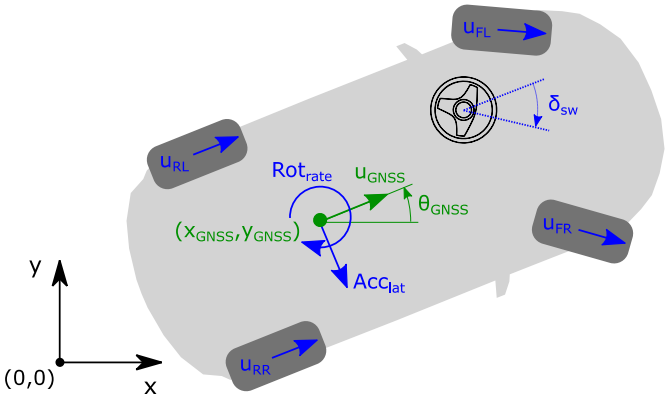

Figure 2. Preprocessed measured variables obtained by the system, to be later employed in the data fusion module. The schematic diagram represents, in blue, the measurements obtained from the on-vehicle sensors for relative positioning and, in green, the measurements provided by the GNSS receiver. The meaning of all the represented variables is explained in Section 2.2.3.

2.2.3. Data fusion

The output variables coming from the preprocessing block (Figure 2) are fed as measurements into the Extended Kalman Filter (Figure 3), which is responsible ~~of~~for performing the data fusion of all these measurements ~~for~~ in order to achiev~~e~~~~ing~~, as its output, an optimal estimation of the system state.

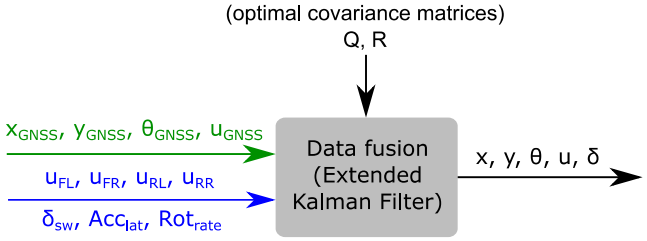

Figure 3. Input (measured) variables for EKF-based data fusion and output (filtered) system state variables. In green, the measurements provided by the GNSS receiver. In blue, the measurements provided by the on-vehicle sensors. In black, the output~~ted~~ system state

variables. The optimal covariance matrices ($\boldsymbol{Q}$ and $\boldsymbol{R}$) are employed to weight the reliability on each individual measurement.

In this article, the Extended Kalman Filter was particularized for the car vehicle system (Figure 4), by introducing the Ackerman steering geometry into the bicycle kinematic model for describing car motion (Jazar, 2014). For completely specifying the car-system state, with regard to its positioning, the bicycle model is here assumed as an approximation. In this scenario, the five variables depicted in Figure 4 are enough to describe the system's kinematic state at a discrete instant *k*. Thus, the positioning-related state of the car system can be fully determined by the set of five variables shown in Equation (1):

$$\mathbf{x}_k = (x_k, y_k, \theta_k, u_k, \delta_k)^T \tag{1}$$

where x_k denotes the UTM position in the X axis or Easting position; y_k denotes the UTM position in the Y axis or Northing position; θ_k denotes the vehicle heading direction with respect to the positive X axis; u_k denotes the speed of the vehicle; and δ_k denotes the angle formed by the virtual front wheel and the vehicle heading ~~direction~~angle.

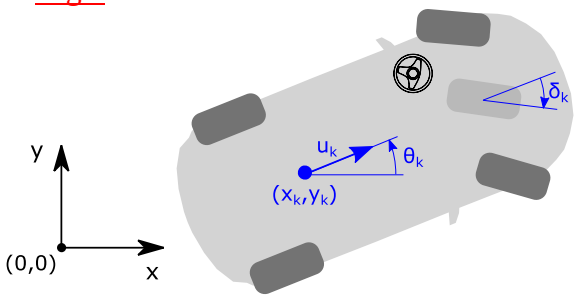

Figure 4. Car-system state variables, where all the variables needed to completely define the kinematic state of the car system are depicted.

In this article, the GNSS receiver and the on-vehicle sensors for relative positioning (Figure 2) provide the measured variables shown in Equation (2):

$$\bar{\mathbf{z}}_k = (x_{GNSS}, y_{GNSS}, \theta_{GNSS}, u_{GNSS}, u_{FL}, u_{FR}, u_{RL}, u_{RR}, \delta_{sw}, Acc_{lat}, Rot_{rate})^T \tag{2}$$

where x_{GNSS} denotes the UTM easting position in the X axis supplied by the GNSS receiver; y_{GNSS} denotes the UTM northing position in the Y axis supplied by the GNSS receiver; θ_{GNSS} denotes the heading direction supplied by the GNSS receiver; u_{GNSS} denotes the speed of the vehicle supplied by the GNSS receiver; u_{FL} denotes the front-left wheel speed; u_{FR} denotes the front-right wheel speed; u_{RL} denotes the rear-left wheel speed; u_{RR} denotes the rear-right wheel speed; δ_{sw} denotes the turning angle of the steering wheel with respect to the equilibrium; Acc_{lat} denotes the lateral or centripetal acceleration; and Rot_{rate} denotes the rotation rate of the vehicle, *i.e.* the rate of change of the heading angle.

The relationships between the system state variables ($\mathbf{x}_k$) and the measurement variables ($\mathbf{z}_k$) were deduced by applying the Ackermann steering geometry (Figure 5) as a good approximation for the car vehicle. A detailed derivation of these relationships can be found in Appendix A.

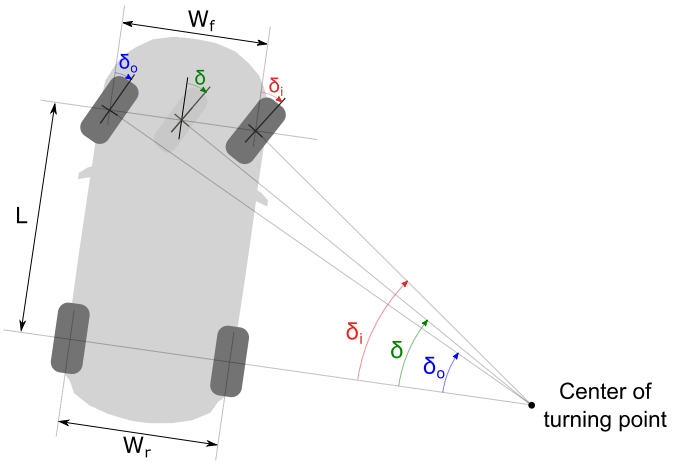

Figure 5. Ackerman steering model.

~~Having~~ Considering these state ($\mathbf{x}_k$) and measurement ($\mathbf{z}_k$) vectors, the concrete particularization of the Extended Kalman Filter yielded the following functions $\boldsymbol{f}$ and $\boldsymbol{h}$~~, respectively,~~ for the state prediction and measurement update, respectively, as shown in Equations (3) and (4):

$$\mathbf{x}_k = \begin{pmatrix} x_k \\ y_k \\ \theta_k \\ u_k \\ \delta_k \end{pmatrix} = \boldsymbol{f}(\mathbf{x}_{k-1}) + \mathbf{w}_{k-1} = \begin{pmatrix} x_{k-1} + \Delta t \cdot u_{k-1} \cdot \cos(\theta_{k-1}) \\ y_{k-1} + \Delta t \cdot u_{k-1} \cdot \sin(\theta_{k-1}) \\ \theta_{k-1} + \Delta t \cdot \dfrac{u_{k-1}}{L} \cdot \tan(\delta_{k-1}) \\ u_{k-1} \\ \delta_{k-1} \end{pmatrix} + \mathbf{w}_{k-1} \tag{3}$$

$$\begin{aligned} \mathbf{z}_k &= (x_{GNSS}, y_{GNSS}, \theta_{GNSS}, u_{GNSS}, u_{FL}, u_{FR}, u_{RL}, u_{RR}, \delta_{sw}, Acc_{lat}, Rot_{rate})^T = \\ &= \boldsymbol{h}(\mathbf{x}_k) + \mathbf{v}_k = \Bigg(x_k,\ y_k, \theta_k, u_k, \frac{\sqrt{(\tan(\delta_k) \cdot L)^2 + \left(L + \tan(\delta_k) \cdot \frac{W_f}{2}\right)^2}}{L} \cdot u_k, \\ &\quad \frac{\sqrt{(\tan(\delta_k) \cdot L)^2 + \left(L - \tan(\delta_k) \cdot \frac{W_f}{2}\right)^2}}{L} \cdot u_k, \left(1 + \frac{W_r \cdot \tan(\delta_k)}{2L}\right) \cdot u_k, \\ &\quad \left(1 - \frac{W_r \cdot \tan(\delta_k)}{2L}\right) \cdot u_k, \delta_k \cdot S_{ratio}, \frac{{u_k}^2}{L} \cdot \tan(\delta_k), \frac{u_k}{L} \cdot \tan(\delta_k) \Bigg)^T + \mathbf{v}_k \end{aligned} \tag{4}$$

where $\mathbf{w}_k \sim N(\mathbf{0}, \boldsymbol{Q})$ is the process noise, following a Gaussian distribution with zero vector mean and covariance matrix $\boldsymbol{Q}$; $\mathbf{v}_k \sim N(\mathbf{0}, \boldsymbol{R})$ is the measurement noise, following a Gaussian distribution with zero vector mean and covariance matrix $\boldsymbol{R}$; L is the distance ~~from~~ between the front ~~to~~ and rear vehicle axles; W_r is the distance between wheels ~~i~~on the rear axle; W_f is the distance between wheels ~~i~~on the front axle; S_{ratio} is the steering ratio, *i.e.* the quotient factor that relates the angle ~~at~~to which the steering wheel is turned ~~by the steering wheel~~ and the angle to which ~~turned by~~ the virtual central front wheel turns as a consequence; and Δt is the time elapsed between two consecutive samples, *i.e.* $\Delta t = t_k - t_{k-1}$ if t_k denotes the time when the k-th sample is obtained.

The EKF implementation requires the calculation of two additional matrices for its underlying operation: $\boldsymbol{F}_k$, the state transition matrix, and $\boldsymbol{H}_k$, the observation matrix. In complex cases, they must be computed numerically, on the fly, at each discrete instant, but as far as this model is concerned, analytical derivations can be ~~easily~~ straightforwardly obtained for both $\boldsymbol{F}_k$ and $\boldsymbol{H}_k$ by computing~~, respectively,~~ the Jacobian matrix of the aforementioned $\boldsymbol{f}$ and $\boldsymbol{h}$ functions, respectively. The results from such calculations are provided in Equation (5) and Equation (6), respectively:

$$\boldsymbol{F}_k = \left.\frac{\partial \boldsymbol{f}}{\partial \mathbf{x}_k}\right|_{\hat{\mathbf{x}}_{k|k}} =$$

$$= \begin{pmatrix} 1 & 0 & -\Delta t \cdot \hat{u}_{k|k} \cdot \sin(\hat{\theta}_{k|k}) & \Delta t \cdot \cos(\hat{\theta}_{k|k}) & 0 \\ 0 & 1 & \Delta t \cdot \hat{u}_{k|k} \cdot \cos(\hat{\theta}_{k|k}) & \Delta t \cdot \sin(\hat{\theta}_{k|k}) & 0 \\ 0 & 0 & 1 & \frac{\Delta t}{L} \cdot \tan(\hat{\delta}_{k|k}) & \Delta t \cdot \frac{\hat{u}_{k|k}}{L} \cdot (1 + \tan^2(\hat{\delta}_{k|k})) \\ 0 & 0 & 0 & 1 & 0 \\ 0 & 0 & 0 & 0 & 1 \end{pmatrix} \quad (5)$$

$$\boldsymbol{H}_k = \left.\frac{\partial \boldsymbol{h}}{\partial \mathbf{x}_k}\right|_{\hat{\mathbf{x}}_{k|k-1}} =$$

$$= \begin{pmatrix} 1 & 0 & 0 & 0 & 0 \\ 0 & 1 & 0 & 0 & 0 \\ 0 & 0 & 1 & 0 & 0 \\ 0 & 0 & 0 & 1 & 0 \\ 0 & 0 & 0 & H_{k,5,4} & H_{k,5,5} \\ 0 & 0 & 0 & H_{k,6,4} & H_{k,6,5} \\ 0 & 0 & 0 & \left(1 + \frac{W_r \cdot \tan(\hat{\delta}_{k|k-1})}{2L}\right) & \frac{W_r \cdot (1 + \tan^2(\hat{\delta}_{k|k-1}))}{2L} \cdot \hat{u}_{k|k-1} \\ 0 & 0 & 0 & \left(1 - \frac{W_r \cdot \tan(\hat{\delta}_{k|k-1})}{2L}\right) & -\frac{W_r \cdot (1 + \tan^2(\hat{\delta}_{k|k-1}))}{2L} \cdot \hat{u}_{k|k-1} \\ 0 & 0 & 0 & 0 & S_{ratio} \\ 0 & 0 & 0 & \frac{2 \cdot \hat{u}_{k|k-1}}{L} \cdot \tan(\hat{\delta}_{k|k-1}) & \frac{\hat{u}_{k|k-1}^{\,2}}{L} \cdot (1 + \tan^2(\hat{\delta}_{k|k-1})) \\ 0 & 0 & 0 & \frac{\tan(\hat{\delta}_{k|k-1})}{L} & \frac{\hat{u}_{k|k-1}}{L} \cdot (1 + \tan^2(\hat{\delta}_{k|k-1})) \end{pmatrix} \quad (6)$$

where:

$$H_{k,5,4} = \frac{\sqrt{\left(L \cdot \tan(\hat{\delta}_{k|k-1})\right)^2 + \left(L + \frac{W_f}{2} \cdot \tan(\hat{\delta}_{k|k-1})\right)^2}}{L},$$

$$H_{k,5,5} = \frac{(1+\tan^2(\hat{\delta}_{k|k-1})) \cdot \left(\left(L^2 + \frac{W_f^{\,2}}{4}\right) \cdot \tan(\hat{\delta}_{k|k-1}) + \frac{L \cdot W_f}{2}\right) \cdot \hat{u}_{k|k-1}}{L\sqrt{\left(L \cdot \tan(\hat{\delta}_{k|k-1})\right)^2 + \left(L + \frac{W_f}{2} \cdot \tan(\hat{\delta}_{k|k-1})\right)^2}},$$

$$H_{k,6,4} = \frac{\sqrt{\left(L\cdot\tan\left(\hat{\delta}_{k|k-1}\right)\right)^2+\left(L-\frac{W_f}{2}\cdot\tan\left(\hat{\delta}_{k|k-1}\right)\right)^2}}{L},$$

$$H_{k,6,5} = \frac{\left(1+\tan^2\left(\hat{\delta}_{k|k-1}\right)\right)\cdot\left(\left(L^2+\frac{{W_f}^2}{4}\right)\cdot\tan\left(\hat{\delta}_{k|k-1}\right)-\frac{L\cdot W_f}{2}\right)\cdot\hat{u}_{k|k-1}}{L\sqrt{\left(L\cdot\tan\left(\hat{\delta}_{k|k-1}\right)\right)^2+\left(L-\frac{W_f}{2}\cdot\tan\left(\hat{\delta}_{k|k-1}\right)\right)^2}}.$$

2.2.4. Tuning

The tuning block is responsible ~~of~~ for feeding the optimal noise covariance matrices (***Q*** and ***R***) to the data fusion module so that it can achieve the best possible results. So far, the proposed system works with static matrices, which are tuned in advance and fixed for every instant of time.

3. Experimental Section for System Performance Evaluation

The real-time system proposed in Section 2 was assessed in post-processing~~,~~ using the setup represented in Figure 6~~, by~~ and following the scheme depicted in Figure 7.

3.1. Materials

The materials employed in the experimental tests of this article were: a low-cost GPS receiver, an accurate high-end GPS receiver, a laptop computer, and a car vehicle with embedded relative positioning sensors available through an OBD-II adapter. Figure 6 shows, schematically, the experimental setup for the tests.

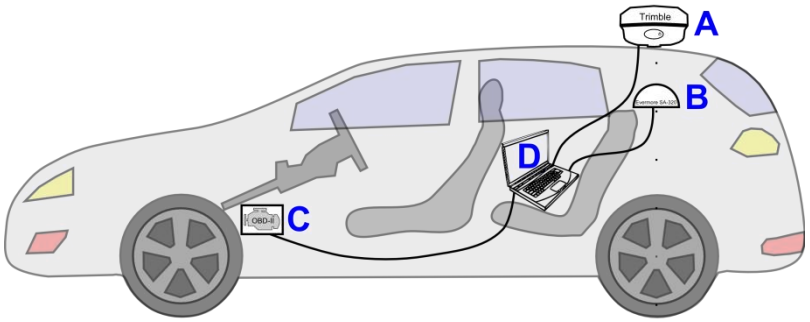

Figure 6. Car schematic outlining the materials setup throughout the experimental tests: (**A**) a *Trimble R4* accurate high-end GPS receiver with RTK corrections, (**B**) an *EverMore SA-320* low-cost GPS receiver, (**C**) an *OBD-II VAG-COM 10.6* adapter, and (**D**) an *Asus K72Jk* laptop computer.

The low-cost GPS receiver was an *EverMore SA-320* with a *SiRFstarIII* chipset, and it was employed to acquire the GPS positions at a 5 Hz sampling rate. The accurate high-end GPS receiver, which ~~acquiring~~ acquired GPS positions at a sampling rate of 1 Hz, was a *Trimble R4* configured to use RTK (Real Time Kinematic) corrections, and it was employed as a ground truth reference~~,~~ so as to assess the precision of the deployed system. The employed RTK corrections were supplied by the *Agro-Food Technological Institute of Castilla y León* (ITACyL) ("Network of GNSS stations of

Castilla y León", 2016). The laptop employed in the tests was an *Asus K72Jk*, and it was used to acquire and store the data from all the connected sensors. Furthermore, the laptop was also used for the subsequent post-processing stages. The car vehicle was a *Seat León MK2*, and it was employed, together with all the sensors on board the car, to perform the tests along real urban area roads in Valladolid, Spain.

The car sensors employed during the tests, as well as the measurements obtained from each of them, were the same as depicted in Figure 1b: (*i*) the G85 sensor, measuring the steering wheel angle (δ_{sw}); (*ii*) the G200 sensor, measuring both the lateral acceleration (Acc_{lat}) as a direct measurement and the vehicle's rotation rate or angular speed (Rot_{rate}) as an indirect measurement; (*iii*) the G47 sensor, measuring the speed of the front left wheel (u_{FL}); (*iv*) the G45 sensor, measuring the speed of the front right wheel (u_{FR}); (*v*) the G46 sensor, measuring the speed of the rear left wheel (u_{RL}); and (*vi*) the G44 sensor, measuring the speed of the rear right wheel (u_{RR}).

3.2. Methods

The stages involved in this article are summarized as: (*i*) data acquisition stage, (*ii*) preprocessing stage, (*iii*) filter tuning stage, (*iv*) data fusion particularization via Extended Kalman Filter, and (*v*) positioning error evaluation. An overview of this whole process is illustrated in Figure 7.

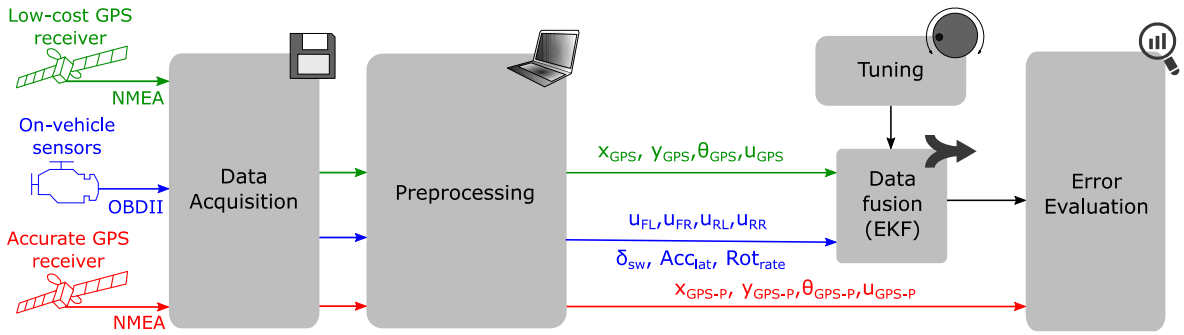

Figure 7. Block diagram summarizing the stages undertaken in the experimental tests for assessing the performance of the proposed system.

3.2.1. Data acquisition stage

First, the data acquisition stage was performed. In this stage, a typical urban path was followed by the ~~car~~ vehicle equipped with ~~while all~~ the aforementioned on-board sensors ~~were equipped on it~~. RMC NMEA 0183 sentences were acquired from both GPS receivers at a sampling rate of 1 Hz and 5 Hz for the high-end and low-cost one, respectively. The accurate GPS receiver employed RTK corrections which were provided by the *Agro-Food Technological Institute of Castilla y León* (ITACyL). For its part, the low-cost GPS receiver did not employ any kind of correction for positioning improvement. During all the recordings, the presence of no outages was ensured in order to keep an accurate reference from the high-end GNSS receiver. Simultaneously, data was obtained from the several relative positioning sensors of the car ~~was obtained~~ through the OBD-II standard by using a *VAG-COM 10.6* connector. The real experimental setup for the tests is shown in Figure 6, and the measurements taken from both sources are depicted in Figure 2.

It is worth mentioning, at this stage, that the heading angle for the *EverMore SA-320* low-cost GPS receiver was obtained in this case from the sixth field (*Track angle in degrees with respect to the True North*) as provided in the RMC NMEA 0183 sentences. Since no built-in compass was available inside the receiver, this value was internally computed from consecutive positions along the followed trajectory.

3.2.2. Preprocessing stage

Second, the preprocessing stage took place. It consisted of the following sub-stages: (*i*) data conversion from geodetic to UTM coordinates and conversion to SI units, (*ii*) resampling stage, (*iii*) synchronization stage, (*iv*) positioning offset elimination. In order to obtain the positions projected ~~i~~onto a 2D map, WGS84 to UTM conversion was first applied ~~first~~ together with units' conversion into SI. After that, the sequence of data was interpolated using piecewise cubic interpolation~~,~~ and resampled, since the data from the diverse sensors was sampled at different rates and even at non-uniform instants of time. In order to keep a high enough temporal resolution, one with the error bounded under 20 milliseconds, a 50 Hz sampling rate was chosen. This way, a new sequence with more samples per second was obtained, making the subsequent synchronization stage easier too. After this processing, the sequences coming from different sensors were synchronized, since the clocks of the different subsystems differed slightly. Last, since the absolute positioning error was left out of the evaluation, the positioning data coming from the *Trimble R4* was spatially aligned with the data ~~in~~ from the low-cost GPS receiver~~,~~ so as to focus ~~just~~ solely on the relative positioning precision of the deployed system.

3.2.3. Filter tuning stage

Third, after having particularized the filter properly, the tuning stage took place. This stage undertook the computation of optimal $\boldsymbol{Q}$ and $\boldsymbol{R}$ noise covariance matrices for the EKF. The optimality criterion employed in this article was the reduction of the error throughout a sample training trajectory. In order to tune the covariance matrices, a hand-tuning approach was employed instead of other feasible alternative tuning techniques (Abbeel, Coates, Montemerlo, Ng, & Thrun, 2005), assuming ~~uncorrelation~~ non-correlation among noise components. This approach was selected since neither reliable nor accurate ground truth reference for the whole system state was available.

3.2.4. Data fusion particularization via *Extended Kalman Filter*

Fourth, the Extended Kalman Filter particularization derived in Subsection 2.2.3 was applied to the preprocessed data. This data fusion stage took as input the preprocessed measured variables~~, coming~~ from the previous stage~~,~~ and produced an optimal estimation of the state variables ~~by~~ using the tuned covariance matrices.

3.2.5. Positioning error evaluation

Finally, in order to assess the improvements offered by the system developed here, positioning distance error with respect to the real path was computed for each point along the trajectory. A

histogram of this error distribution was obtained before and after fusing the data, from which the Root Mean Square Error (RMSE) value, the 95*th*-percentile of the error distribution, and the maximum error value were calculated as statistical parameters.

4. Results

After having performed all the aforementioned stages (Section 3.2), the following results were obtained.

4.1. Tuning of Q and R covariance matrices

The ~~hand-tuned~~ optimal covariance matrices, obtained in the experimental tests following the hand-tuning process explained in Section 3.2.3, are shown in Equation (7).

$$\boldsymbol{Q} = diag\left(10^{-8}\, m^2, 10^{-8}\, m^2, 10^{-12}\, rad^2, 10\, \frac{m^2}{s^2}, 50\, rad^2\right)$$

$$\boldsymbol{R} = diag\left(1.15\, m^2, 1.75\, m^2, 0.1\, rad^2, 0.0125\, \frac{m^2}{s^2}, 0.45\, \frac{m^2}{s^2}, 0.45\, \frac{m^2}{s^2}, 0.45\, \frac{m^2}{s^2}, \right. \tag{7}$$

$$\left. 0.45\, \frac{m^2}{s^2}, 10^{-8}\, rad^2, 0.01\, \frac{m^2}{s^4}, 10^{-5}\, \frac{rad^2}{s^2}\right)$$

It is worth remarking that the units of measurement for each component in Equation (7) are those of the corresponding variable squared. Since the optimal matrices are diagonal, *i.e.* noise non-correlation between variables was assumed here, all non-zero elements in the covariance matrices simply represent variances.

The optimal covariance matrix $\boldsymbol{Q}$, shown in Equation (7), evinces a high confidence in the prediction for both X and Y positions as well as for the heading angle. This seems to be reasonable, since no sudden changes in heading are expected to happen at the relatively high 50 Hz sampling rate. Therefore, in this case, the prediction given by the bicycle kinematic model is a very precise approximation. On the other hand, as shown by the high values of those components in matrix $\boldsymbol{Q}$, assuming constant speed and constant steering angle does not lead to reliable hypotheses, since accelerations and turnings are likely to occur in a normal trajectory described by the car. Meanwhile, regarding the uncertainties for each measurement provided in the optimal covariance matrix $\boldsymbol{R}$, it is worth highlighting the high accuracy of the steering wheel angle, lateral acceleration, and rotation rate measurements obtained from the on-vehicle sensors. On the other hand, the speedometer-based measurements are less accurate than expected since the Electronic Control Unit (ECU) in the car provided speeds with a resolution of 1 km/h. Moreover, an increment in uncertainty for those measurements arose due to the imperfect matching between the expected Ackermann steering geometry and the actual one from the real car. It is also worth highlighting that the estimated variances for the GNSS-supplied X and Y positions are lower than expected due to three reasons: (*i*) the absolute positioning error being left out of consideration in this study, by artificially removing it beforehand in order to perform just the assessment in terms of relative positioning improvements, (*ii*) the non-Gaussianity of the actual positioning error distribution while assuming additive Gaussian noise for the EKF, and (*iii*) the EKF tuning process underestimating the GNSS positioning noise variances, since it

is the only source of absolute positioning, and thus avoiding the inherent drifting apart due to an overconfidence in the remaining inertial sensors. Furthermore, the discrepancy between variances for the X and Y positions is explained by considering the function of the UTM projection as well as the particular geometric configuration of the GPS satellite constellation, *i.e.* Geometric Dilution Of Precision (GDOP), when the experiments were recorded.

4.2. Visual positioning improvements

The resulting trajectory after filtering, making use of the aforementioned matrices (Section ~~3~~4.1), is shown in Figure 8. A greater, qualitatively significant, similarity can be appreciated between the trajectories after applying the data fusion (blue) as compared to the one just based on the low-cost GNSS data (red) with respect to the ground truth reference (green).

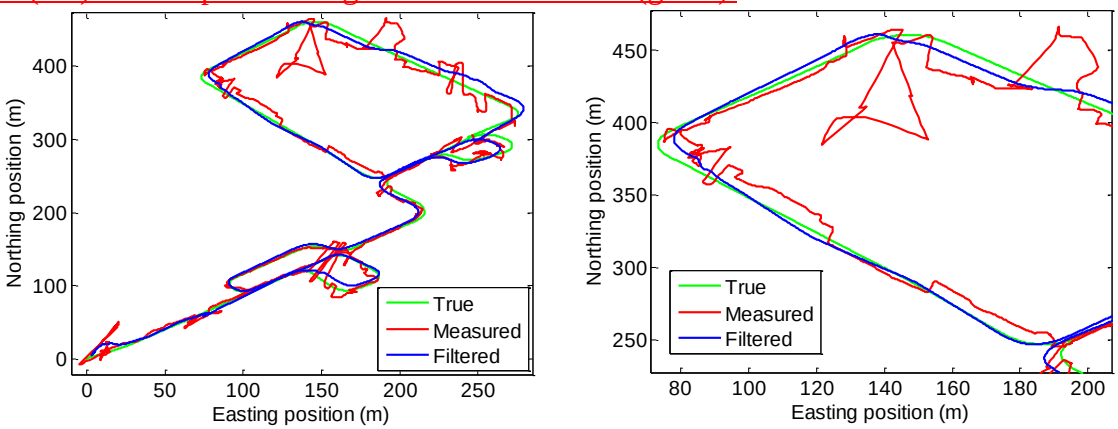

(**a**) (**b**)

Figure 8. (**a**) UTM projection of the 1.5-kilometer-long test road path, and (**b**) a close-up of a region of interest (road intersection and turnarounds).

4.3. Positioning error reduction quantification

Figure 9 presents the distance error histogram with ~~regard~~ respect to real reference positions, before and after using the here-proposed system. It is observed that, before applying the proposed data fusion system, there are distance errors of up to 80 m (Figure 9a) whereas, after applying it, the distance errors do not go any higher than 21 m (Figure 9b).

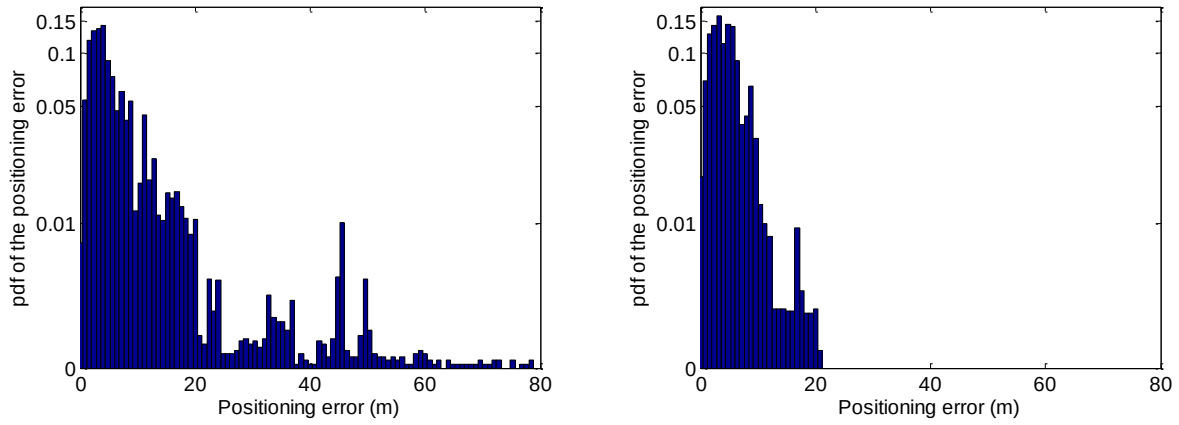

Figure 9. Histogram of distance errors: (**a**) before applying the proposed data fusion system, and (**b**) after applying the proposed data fusion system. The histogram has been normalized so that it has a unitary area, representing an approximation to the probability density function (*pdf*) of the distance errors statistical random variable. Note that the Y-axis is not linear since μ-law companding algorithm, with a value of μ equal to 511, has been used in order to better show differences before and after applying the proposed data fusion system.

The RMS value, the 95*th*-percentile, and the maximum were computed, on the basis of the statistical distribution of the distance errors shown in Figure 9. These measurements can be employed to quantify the error improvement achieved by the proposed data fusion system. Table 1 shows these statistical parameters obtained from the distance error distribution, as well as the error reduction, computed as in Equation (8):

$$Error\ reduction\ (\%) = \frac{error\_before - error\_after}{error\_before} \times 100 \quad (8)$$

The maximum error was bounded below 21 meters after applying the proposed method, as compared to the previous 80 meters bound. Similarly, the RMSE and the 95*th*-percentile of distance error were reduced by roughly 50%. This result poses strong evidence of the quality of the ~~here proposed~~ data fusion system proposed by this study.

Table 1. Statistical parameters of the distribution of distance errors, before and after applying the proposed data fusion system, in the trajectory used for real tests shown in Figure 8.

	Before	**After**	**Error reduction**
Distance Root-Mean Square Error (RMSE) (m)	11.6560	5.7427	50.73 %
95*th*-percentile of distance error (m)	20.0	9.6	52 %
Maximum distance error (m)	78.5859	20.4732	73.95 %

5. Discussion

The main finding of this study is that on-vehicle sensors data can be employed through the proposed data fusion system for improving the car positioning precision provided by a standalone low-cost GNSS receiver. The positioning precision improvement can reach up to 50% in terms of the RMSE, 50% in terms of the 95*th*-percentile of the distance error distribution, and 75% in terms of the maximum distance error.

The aforementioned finding is supported by the results presented in Section 4, specifically by Figure 8, Figure 9, and Table 1. Figure 8 qualitatively shows the positioning precision improvements ~~posed~~ arising from the use ~~by~~ of the proposed data fusion system.~~,~~ ~~obtaining a~~A significantly closer trajectory to the real one can be obtained after applying th~~e proposed data fusion~~is system. Figure 9 depicts the histogram of the errors before and after performing data fusion. As can be ~~appreciated~~ seen in these histograms (Figure 9), the data fusion system achieves a shifting to the left in the errors distribution, having no errors greater than 21 meters after performing data fusion (Figure 9b)~~;~~, in contrast, ~~while~~ the maximum errors reached 80 meters ~~in~~ when the low-cost GPS receiver was used on its own (Figure 9a). Table 1 shows that, with respect to when the GPS receiver was used on its own, the positioning error reductions ~~, with respect to solely using the GPS receiver by itself,~~ were 50.73%, 52%, and 73.95% in terms of the RMSE, the 95*th*-percentile of the distance error distribution, and the maximum distance error, respectively. These results provide evidence of the feasibility of employing the proposed data fusion system to improve car positioning precision when using low-cost GNSS receivers. Moreover, it is expected that the proposed system could be of great value in the event of short-term GNSS signal outages, which are prevalent in cities with tall buildings and skyscrapers.

The results of this article are in line with previous research regarding on-vehicle sensors and GNSS data fusion, despite the fact that most of the reviewed ~~previous~~ articles use different data fusion approaches. The article written by Bonnifait *et al.* (Bonnifait, et al., 2001) proposes a multi-stage EKF-based system that first performs an odometry-based path reconstruction and then fuses its results with the GNSS-based path. In terms of positioning error reduction, ~~Significant~~ significant local improvements~~, in terms of positioning error reduction,~~ are found in this article, although they do not seem to be consistent over time. El Najjar and Bonnifait's article (El Najjar & Bonnifait, 2005) proposes an EKF-based data fusion system of DGPS (Differential GPS) and ABS sensor measurements, which is complemented by a novel road-matching method based on the belief theory. By also using a map-matching technique, this data fusion approach is able to further reduce positioning errors, making this approach viable and useful when no GNSS data is available for long periods of time. In Gning and Bonnifait's article (Gning & Bonnifait, 2005), they propose a data fusion scheme based on Forward and Backward Propagation constraints for GNSS, two ABS rear wheel speed sensors, and gyroscope data. Their results show~~ed~~ that EKF-based data fusion outperforms their novel proposed technique. The article written by Song *et al.* (Song, et al., 2014) proposes a novel hybrid multi-sensor fusion strategy for positioning vehicles in tunnels based on Radio Frequency Identification (RFID) tags and on-vehicle sensors. Due to use of the short-range RFID technology, great improvements in positioning precision are achieved by this strategy. However, its huge associated cost of deployment, requiring the presence of RFID tags every 6 meters, makes this approach currently unfeasible for widespread use in real life applications other than tunnels.

The system proposed in this article is a new contribution for two main reasons. The first reason is that the model employed to describe the state of car systems~~, up to the authors' knowledge,~~ has not been previously used, so far as the authors are aware. Other articles (Bonnifait, et al., 2001; El Najjar & Bonnifait, 2005; Gning & Bonnifait, 2005) have used both the angle rotated by the vehicle between consecutive samples, *i.e.* the change in the vehicle's heading direction, and the turning radius as intermediate variables, but the ~~employed~~ new proposed model avoids using any intermediate variable. This way, data fusion in this article is performed ~~employing~~ requiring less overall variables. It is expected that this reduction in the necessary number of variables will translate into a lower computational load associated with the EKF-based data fusion. The second reason is that the proposed system performs positioning data fusion as a single EKF-based stage and is, thus, more flexible to the addition of new on-vehicle sensors as input or measured data. It is also expected that this reduction in the number of EKF-based stages will imply, once again, less computational load for the whole proposed system while not being detrimental in terms of precision.

One strength of the proposed system is its low implementation cost for most modern car vehicles. Two reasons can be highlighted for this claimed low-cost design: (*i*) today, most cars have all the necessary information to implement this system, with GNSS receivers on-board and many on-vehicle sensors available through the CAN bus of the vehicle; and (*ii*) modern car vehicles have an embedded on-board computer (Powertrain Control Module, PCM), so the software needed to combine all this information and estimate the position can be deployed in the embedded PCM. Taking these reasons into account, it will be possible to implement the proposed system for improving the car positioning precision without needing any additional hardware. Another strength of the proposed system is that, by its design, it can be adapted to incorporate more sensors, such as longitudinal accelerometers and wheel steering angle sensors, with greater ease.

The main weakness of this study lies in its not having contrasted the results with several low-cost GNSS receivers. Nevertheless, this weakness is not a significant issue since the low-cost GPS receiver employed in this article can be considered as an archetypical low-cost GPS receiver, ~~being~~ which is representative of the main alternatives in the market. Moreover, the main performance benefits of the proposed system are expected to be reached during short-time GNSS signal outages, thus achieving significant precision improvements in those situations, even for high-end GNSS receivers. Although more precise techniques have been developed for enhancing the positioning provided by low-cost GNSS receivers, *e.g.* single-frequency Precise Point Positioning (PPP) (Chen & Gao, 2005), in the event of outages the proposed system would still be useful for improving vehicle's positioning. A second weakness is the fact that all experimental tests were performed in the same location (Valladolid, Spain). However, this weakness is also not a significant issue since it is expected that~~, in other urban areas,~~ the behavior will be similar in other urban areas. Furthermore, the proposed system is expected to behave even better in urban environments with taller buildings than the ones present in Valladolid (Spain). A third weakness of this article is the way the real-time system was evaluated in post-processing. Nonetheless, this weakness is also not a significant issue. Other articles from the literature have also assessed real-time systems in post-processing in a similar fashion (Bonnifait, et al., 2001; Gning & Bonnifait, 2005). Moreover, the alleged real-time capabilities of the proposed system have been checked, revealing that the real-time constraints can be guaranteed. In the conducted tests, it took less than 8 seconds to execute 260 seconds of data in a MATLAB® implementation running ~~i~~on

an *Asus K72Jk* laptop. This fact reveals that, were this system to be deployed in a microprocessor-based device such as *Raspberry Pi 3*, it would be perfectly able to work in real-time, performing ~~the whole~~all the related processing in a bounded time before the subsequent data samples are available. Another weakness of the proposed data fusion system lies in the use of the not-perfectly-valid assumption, inherent to the Extended Kalman Filter, that the underlying noise is Gaussian. Other non-linear filtering techniques, such as the particle filter, could further improve the results of the proposed system by avoiding this assumption. Nevertheless, due to their associated higher computational load, they were discarded so as to meet the real-time constraints when executed in low-cost computing platforms.

~~Three~ Five main possible future lines, ~~in~~ some of which the authors are already working in, have been detected for extending this article's work. A first future line of research could undertake the inclusion of map information into the model, by avoiding the fact that the position lies within prohibited locations such as buildings or sidewalks, to further improve the car positioning precision. A second future line of research could consider the extension of the proposed system to be able to function even when no GNSS data is available for prolonged periods of time, also undertaking the precision and performance assessment of that future system during both short-term and long-term GNSS signal outages. A third future line of research could tackle the dynamic tuning of the covariance matrices involved in the EKF for data fusion, by characterizing the sensors accuracy and using the Dilution ~~of~~ Of Precision (DOP) information from the GNSS constellation, to further improve the car positioning precision. A fourth future line of research could execute a fair performance comparison of the most remarkable state-of-the-art data fusion systems for improving car positioning precision, thus providing insightful advantages and disadvantages of each method, both theoretically and experimentally. A fifth future line of research could focus on integrating the proposed data fusion system into existing expert systems used in autonomous cars, probably including additional sensors for relative and absolute positioning, evaluating its suitability for self-driving in an experimental environment.

6. Conclusions

The main contribution of this work is the proposal of a novel system that enables keeping an accurate car positioning during GNSS signal outages while being simpler and more flexible to the incorporation of new sensors into it, as compared to other existing alternatives. The proposed data fusion system for car vehicles, which fuses data from a low-cost GNSS receiver with data from other on-vehicle sensors for relative positioning, can reduce the positioning error with respect to the positioning error of the low-cost GNSS receiver alone. This reduction can reach up to 50% in terms of the RMSE, 50% in terms of the 95*th*-percentile of the distance error distribution, and 75% in terms of the maximum distance error. The best precision improvements are achieved in urban areas, where tall buildings hinder the effectiveness of GNSS systems. Future work, tackling the dynamic tuning of the covariance matrices or incorporating additional sensors and map information into the model, among other possibilities, could further improve the performance of the here-proposed system, enabling a more accurate functioning even for prolonged periods of GNSS signal outages.

Acknowledgments

The work made in this article by Ruben Ruiz-Gonzalez was possible thanks to a "*Formación de Personal Investigador*" doctoral program grant, financed by the *Universidad de Valladolid* (Spain) and co-financed by *Banco Santander*.

The authors would like to express their sincere gratitude to Dr. Víctor Martínez-Martínez for his valuable, expert help and advice along all the stages of this study. The authors are also grateful for the helpful comments given by two anonymous reviewers on a previous draft of this manuscript. Furthermore, the authors want to acknowledge the valuable help provided with the language editing and proofreading of the article provided by the Writing Center of the University of Kentucky (USA), with a special mention to Jillian Winter and Leslie C. Davis.

Appendix A.—Derivation of relationships between state and measured variables for a car vehicle

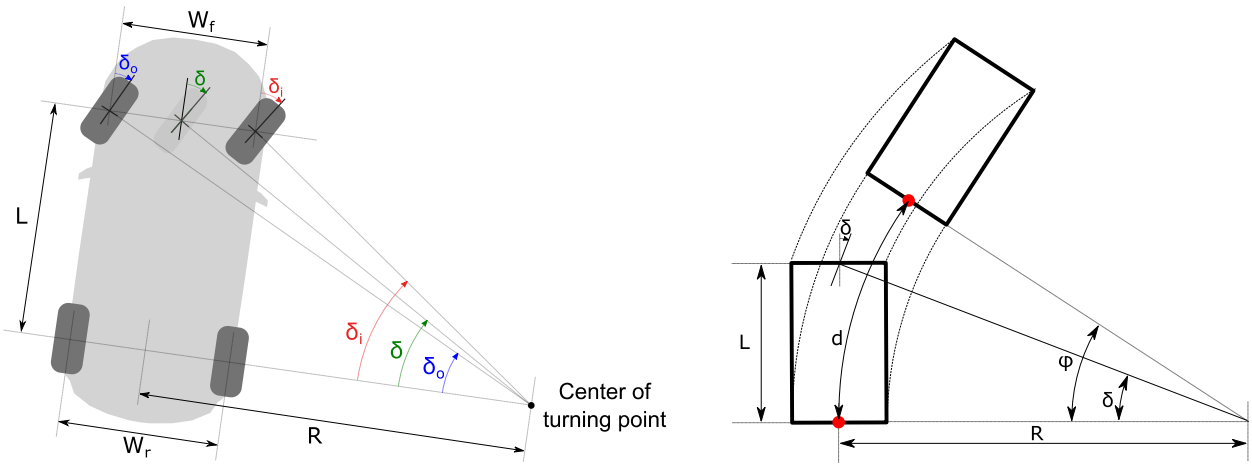

(**a**) (**b**)

Figure A.1. (**a**) Ackerman steering geometry, showing the relationship between the angle turned by each front wheel and the virtual central wheel used in the bicycle model. The "i" and "o" subscripts denote, respectively, the inner and outer front wheels with respect the center of turning point. For clockwise turns, the inner and outer wheels are, respectively, the front-right and front-left wheels, and vice versa for counter-clockwise turns. (**b**) Displacement between two consecutive samples, considering a time lapse short enough to assume a circular movement.

In this appendix, a formal derivation of the relationships between state and measured variables is provided.

Let us first introduce the notation and nomenclature employed throughout this appendix. Let us denote with subscripts FL, FR, RL, and RR, respectively, whenever we refer to the front left, front right, rear left, and rear right wheels. Let us continue with some definitions in Figure A.1: L denotes the distance between the rear and front axles of the car vehicle; W_r denotes the length of the rear axle of the car; W_f denotes the length of the front axle of the car; R denotes the instantaneous turning radius of the central point in the rear axle; φ denotes the angle turned between two consecutive samples; δ

denotes the equivalent angle turned by the virtual wheel used for the bicycle model; and d denotes the distance travelled between two consecutive samples by the central point of the rear axle of the car.

After having introduced the notation, and before starting with the derivations, a sign criterion for δ must be defined. In this article, δ is positive if clockwise and negative otherwise. Thus, in clockwise or right turns, δ is positive. In counter-clockwise or left turns, δ is negative.

Assuming the Ackerman steering geometry for the car vehicle, all four wheels turn with respect to the same turning point (Figure A.1a). ~~This way~~In turn, all the wheels move in such a way that they locally describe a circular trajectory, turning the same angle with respect to the turning point (Figure A.1b).

Taking into account all the aforementioned considerations, we can now proceed to the derivations.

From basic trigonometry on rectangle triangles in Figure A.1, it becomes obvious that:

$$R = \frac{L}{\tan \delta} \tag{A.1}$$

Assuming, in Figure A.1b, constant speed for the car vehicle between consecutive samples, the distance (d) travelled by the central point of the rear axle of the car vehicle (marked as a red point in Figure A.1b) is:

$$d = u \cdot \Delta t = R \cdot \varphi \tag{A.2}$$

where u denotes the car's speed, measured in the central point of the rear axle, and Δt is the time lapse between two consecutive samples.

Solving for u and $\frac{u}{R}$ in Equation (A.2), we get:

$$u = \frac{R \cdot \varphi}{\Delta t} \rightarrow \frac{u}{R} = \frac{\varphi}{\Delta t} \tag{A.3}$$

From Figure A.1b, analogously to the case of the central point of the rear axle derived in Equation (A.2), the distance travelled by each wheel between two consecutive samples is given by:

$$d_{FL} = u_{FL} \cdot \Delta t = R_{FL} \cdot \varphi \tag{A.4}$$

$$d_{FR} = u_{FR} \cdot \Delta t = R_{FR} \cdot \varphi \tag{A.5}$$

$$d_{RL} = u_{RL} \cdot \Delta t = R_{RL} \cdot \varphi \tag{A.6}$$

$$d_{RR} = u_{RR} \cdot \Delta t = R_{RR} \cdot \varphi \tag{A.7}$$

Rearranging Equations (A.4)-(A.7), solving for the wheel speeds, and also using Eqs. (A.1) and (A.3), the speed of each wheel is given by:

$$u_{FL} = \frac{R_{FL} \cdot \varphi}{\Delta t} = \frac{R_{FL}}{R} u = \frac{R_{FL} \cdot \tan(\delta)}{L} u \tag{A.8}$$

$$u_{FR} = \frac{R_{FR} \cdot \varphi}{\Delta t} = \frac{R_{FR}}{R} u = \frac{R_{FR} \cdot \tan(\delta)}{L} u \tag{A.9}$$

$$u_{RL} = \frac{R_{RL} \cdot \varphi}{\Delta t} = \frac{R_{RL}}{R} u = \frac{R_{RL} \cdot \tan(\delta)}{L} u \tag{A.10}$$

$$u_{RR} = \frac{R_{RR} \cdot \varphi}{\Delta t} = \frac{R_{RR}}{R} u = \frac{R_{RR} \cdot \tan(\delta)}{L} u \tag{A.11}$$

The turning radius for each wheel, *i.e.* the distance from each wheel to the center of turning point, can be computed from Figure A.1 by using Pythagoras' theorem, as:

$$R_{FL} = \sqrt{L^2 + \left(R + \frac{W_f}{2}\right)^2} = \sqrt{L^2 + \left(\frac{L}{\tan\delta} + \frac{W_f}{2}\right)^2} \tag{A.12}$$

$$R_{FR} = \sqrt{L^2 + \left(R - \frac{W_f}{2}\right)^2} = \sqrt{L^2 + \left(\frac{L}{\tan\delta} - \frac{W_f}{2}\right)^2} \tag{A.13}$$

$$R_{RL} = R + \frac{W_r}{2} = \frac{L}{\tan\delta} + \frac{W_r}{2} \tag{A.14}$$

$$R_{RR} = R - \frac{W_r}{2} = \frac{L}{\tan\delta} - \frac{W_r}{2} \tag{A.15}$$

Introducing Equations (A.12)-(A.15) in Equations (A.8)-(A.11), we get:

$$u_{FL} = \frac{R_{FL} \cdot \tan(\delta)}{L} u = u \frac{\tan(\delta)}{L} \sqrt{L^2 + \left(\frac{L}{\tan\delta} + \frac{W_f}{2}\right)^2} \tag{A.16}$$

$$u_{FR} = \frac{R_{FR} \cdot \tan(\delta)}{L} u = u \frac{\tan(\delta)}{L} \sqrt{L^2 + \left(\frac{L}{\tan\delta} - \frac{W_f}{2}\right)^2} \tag{A.17}$$

$$u_{RL} = \frac{R_{RL} \cdot \tan(\delta)}{L} u = u \frac{\tan(\delta)}{L} \left(\frac{L}{\tan\delta} + \frac{W_r}{2}\right) \tag{A.18}$$

$$u_{RR} = \frac{R_{RR} \cdot \tan(\delta)}{L} u = u \frac{\tan(\delta)}{L} \left(\frac{L}{\tan\delta} - \frac{W_r}{2}\right) \tag{A.19}$$

Operating further in Equations (A.16)-(A.19), in order to avoid indeterminations caused by divisions by zero when $\delta = 0$, we finally get:

$$u_{FL} = \frac{\sqrt{(\tan(\delta) \cdot L)^2 + \left(L + \tan(\delta) \cdot \frac{W_f}{2}\right)^2}}{L} \cdot u \tag{A.20}$$

$$u_{FR} = \frac{\sqrt{(\tan(\delta) \cdot L)^2 + \left(L - \tan(\delta) \cdot \frac{W_f}{2}\right)^2}}{L} \cdot u \tag{A.21}$$

$$u_{RL} = \left(1 + \frac{W_r \cdot \tan(\delta)}{2L}\right) \cdot u \tag{A.22}$$

$$u_{RR} = \left(1 - \frac{W_r \cdot \tan(\delta)}{2L}\right) \cdot u \tag{A.23}$$

Focusing now on the lateral acceleration, assuming that the speed in the center of mass of the car and that the radius to the center of turning point ~~is~~ are approximately the same as in the central point of the rear axle, it can be computed as:

$$Acc_{lat} = \frac{u^2}{R} = \frac{u^2}{L} \tan(\delta) \tag{A.24}$$

This previous approximation could be easily avoided and corrected for each particular car vehicle model by identifying the exact location of the center of mass for that specific car vehicle.

Additionally, the rotation rate of the car vehicle can be computed as the quotient of the angle turned by the car vehicle in the time lapse between two consecutive samples and this elapsed time. Thus, by using this definition along with Equations (A.1) and (A.3), we get:

$$Rot_{rate} = \frac{\varphi}{\Delta t} = \frac{u}{R} = \frac{u}{L} \cdot \tan(\delta) \tag{A.25}$$

The remaining relationship, between the steering wheel angle (δ_{sw}) and the turning angle of the virtual wheel (δ), is deduced by assuming a linear relationship between them. This assumption is usually correct in modern vehicles, so the quotient relationship between them is given by the steering ratio S_{ratio}. Thus, we have:

$$\delta_{sw} = S_{ratio} \cdot \delta \tag{A.26}$$

To conclude this ~~section~~appendix, it is worth noting that all the derivations made in this section, though just derived while turning clockwise, are valid for both clockwise and counter-clockwise turns. The criterion for the sign of δ captures the information of the turning direction, adapting all the equations and making them valid in both cases.

References

H. W. Sorenson, (Ed.). (1985). *Kalman Filtering: Theory and Application*: IEEE Press.

E. D. Kaplan & C. J. Hegarty, (Eds.). (2005). *Understanding GPS: Principles and Applications* (2nd ed.): Artech House.

Robert Bosch GmbH, (Ed.). (2007). *Bosch Automotive Electrics and Automotive Electronics* (5th ed.): Springer Fachmedien Wiesbaden.

A. H. Jazwinski, (Ed.). (2007). *Stochastic Processes and Filtering Theory*: Dover Publications.

Abbeel, P., Coates, A., Montemerlo, M., Ng, A. Y., & Thrun, S. (2005). Discriminative training of Kalman filters. In *Proceedings of Robotics: Science and Systems*. Cambridge, Massachusetts: MIT Press.

Abbott, E., & Powell, D. (1999). Land-vehicle navigation using GPS. *Proceedings of the IEEE, 87*, 145-162.

Bonnifait, P., Bouron, P., Crubille, P., & Meizel, D. (2001). Data fusion of four ABS sensors and GPS for an enhanced localization of car-like vehicles. In *Robotics and Automation, 2001. Proceedings 2001 ICRA. IEEE International Conference on* (Vol. 2, pp. 1597-1602 vol.1592).

Chen, K., & Gao, Y. (2005). Real-time precise point positioning using single frequency data. In *Proceedings of the 18th International Technical Meeting of the Satellite Division of The Institute of Navigation, ION GNSS 2005* (Vol. 2005, pp. 1514-1523).

El Najjar, M. E., & Bonnifait, P. (2005). A Road-Matching Method for Precise Vehicle Localization Using Belief Theory and Kalman Filtering. *Autonomous Robots, 19*, 173-191.

French, G. T. (1996). *Understanding the GPS: An Introduction to the Global Positioning System* (1st ed.): GeoResearch, Inc.

Gning, A., & Bonnifait, P. (2005). Dynamic Vehicle Localization using Constraints Propagation Techniques on Intervals A comparison with Kalman Filtering. In *Proceedings of the 2005 IEEE International Conference on Robotics and Automation* (pp. 4144-4149).

Gomez-Gil, J., Ruiz-Gonzalez, R., Alonso-Garcia, S., & Gomez-Gil, F. (2013). A Kalman Filter Implementation for Precision Improvement in Low-Cost GPS Positioning of Tractors. *Sensors, 13*, 15307.

Jazar, R. N. (2014). Steering Dynamics. In *Vehicle Dynamics: Theory and Application* (pp. 387-495). New York, NY: Springer New York.

Leung, K. T., Whidborne, J. F., Purdy, D., & Barber, P. (2011). Road vehicle state estimation using low-cost GPS/INS. *Mechanical Systems and Signal Processing, 25*, 1988-2004.

Lin, C.-F. (1991). *Modern navigation, guidance, and control processing* (Vol. 2): Prentice Hall Englewood Cliffs.

Mintsis, G., Basbas, S., Papaioannou, P., Taxiltaris, C., & Tziavos, I. N. (2004). Applications of GPS technology in the land transportation system. *European Journal of Operational Research, 152*, 399-409.

Network of GNSS stations of Castilla y León. Available online: http://gnss.itacyl.es (accessed on 6 June 2016).

Pérez, J., Gonzalez, D., Milanés, V., Perallos, A., Hernandez-Jayo, U., Onieva, E., & García-Zuazola, I. J. (2015). Vehicle Control in ADAS Applications. In *Intelligent Transport Systems* (pp. 206-219): John Wiley & Sons, Ltd.

Schleicher, D., Bergasa, L. M., Ocaña, M., Barea, R., & López, E. (2010). Low-cost GPS sensor improvement using stereovision fusion. *Signal Processing, 90*, 3294-3300.

Song, X., Li, X., Tang, W., Zhang, W., & Li, B. (2014). A Hybrid Positioning Strategy for Vehicles in a Tunnel Based on RFID and In-Vehicle Sensors. *Sensors, 14*.

Tin Leung, K., Whidborne, J. F., Purdy, D., & Dunoyer, A. (2011). A review of ground vehicle dynamic state estimations utilising GPS/INS. *Vehicle System Dynamics, 49*, 29-58.

Titterton, D., & Weston, J. L. (2004). *Strapdown inertial navigation technology* (Vol. 17): IET.

Highlights

- Data fusion with on-vehicle sensor data improves GNSS positioning precision.
- Best precision improvements are achieved while using the system in urban areas.
- The system can be deployed with a low implementation cost in modern car vehicles.
- The system can be easily adapted to incorporate more on-vehicle sensors.